Korean Journal of Remote Sensing, Vol.34, No.4, 2018, pp.649~659
http://dx.doi.org/10.7780/kjrs.2018.34.4.7
ISSN 1225-6161 ( Print )
ISSN 2287-9307 (Online)

Article

# Vicarious Calibration-based Robust Spectrum Measurement for Spectral Libraries Using a Hyperspectral Imaging System

**Junhwa Chi** *†
*Unit of Arctic Sea-Ice Prediction, Korea Polar Research Institute

**Abstract :** The aim of this study is to develop a protocol for obtaining spectral signals that are robust to varying lighting conditions, which are often found in the Polar regions, for creating a spectral library specific to those regions. Because hyperspectral image (HSI)-derived spectra are collected on the same scale as images, they can be directly associated with image data. However, it is challenging to find precise and robust spectra that can be used for a spectral library from images taken under different lighting conditions. Hence, this study proposes a new radiometric calibration protocol that incorporates radiometric targets with a traditional vicarious calibration approach to solve issues in image-based spectrum measurements. HSIs obtained by the proposed method under different illumination levels are visually uniform and do not include any artifacts such as stripes or random noise. The extracted spectra capture spectral characteristics such as reflectance curve shapes and absorption features better than those that have not been calibrated. The results are also validated quantitatively. The calibrated spectra are shown to be very robust to varying lighting conditions and hence are suitable for a spectral library specific to the Polar regions.

Key Words : Hyperspectral imaging, Illumination robustness, Imaging spectroscopy, Spectral library, Vicarious calibration

## 1. Introduction

Recent advances in remote sensing (RS), motivated by a desire to detect and characterize detailed information about targets, have led to the development of advanced sensors that acquire extremely detailed spectral signatures. Hyperspectral imaging or image (HSI), also known as imaging spectroscopy, is a relatively new technology that was developed in the laboratory by physicists and chemists over the past century to detect individual absorption features related to specific chemical bonds in a solid, liquid, or gas (Clark, 1999; Martin and Aber, 1997). HSI has gained increasing attention in many RS applications that have focused on the Earth during the past decade because of its ability to record reflected radiation from a ground target over a continuous range of contiguous bands. High spectral resolution sensors, which often acquire

Received August 7, 2018; Revised August 21, 2018; Accepted August 22, 2018; Published online August 24, 2018
† Corresponding Author: Junhwa Chi (jhchi@kopri.re.kr)

data in at least 100 spectral bands with narrow bandwidths (5-10 nm), provide better material identification ability than multispectral sensors (Solomon, 1985).

In recent years, airborne and spaceborne sensors such as AVIRIS (Airborne Visible/Infrared Imaging Spectrometer), Hyperion, and EnMAP (Environmental Mapping and Analysis Program) have become relatively common, and many methods facilitate the utilization of data from these sensors. Moreover, the development of very small HSI sensors and unmanned aerial vehicle (UAV) technologies has improved accessibility to HSI data (Chi and Crawford, 2014; Green *et al*., 2003; Habib *et al*., 2016; Habib *et al*., 2017; Hruska *et al*., 2012). However, it is difficult to derive precise spectra from image pixels using aerial HSI sensors because a mixture of more than one spectral signature is associated with different classes. This limitation is mostly attributed to the low spatial resolution of a sensor, and the effects multiple sources of interference along with atmospheric attenuation, varying illumination conditions, sensor geometry, and multiple scattering, which are difficult to model and remove (Adams *et al*., 1986; Keshava and Mustard, 2002; Segl *et al*., 2010). Thus, because of the cost, risk, and limitations of aerial platforms, ground-based hyperspectral data are often acquired under controlled conditions such as a laboratory or in the field to obtain robust and accurate target spectral information.

A spectral library is a set of digital reflectance spectra measured in the laboratory or from air/spacecraft. It was developed to support imaging spectroscopy studies of the Earth and other planets (Clark *et al*., 1993). The library includes the spectra of natural materials (e.g., rocks, minerals, soils, vegetation, snow, and ice) and manmade materials and includes wavelengths from visible light to short-wavelength infrared (Baldridge *et al*., 2009; Clark *et al*., 1993). In a quantitative analysis of RS data, the spectral library plays an important role in identifying the components in a spectrum of an unknown target and quantifying the components in a mixed pixel. Moreover, it is often used as reference data for radiometric calibration to maintain the radiometric quality of RS images. Although the library includes many contributions from the Advanced Spaceborne Thermal Emission Reflection Radiometer (ASTER), the Jet Propulsion Laboratory (JPL), Johns Hopkins University, and the United States Geological Survey (USGS), they were mostly developed in mid-latitude regions. Because ecosystems and landcover types in the Arctic and Antarctic are quite different from mid-latitude regions, the current libraries may not be appropriate for the environment of the Polar regions. Only limited research has been undertaken to develop a spectral library for the Polar regions. Goswami and Matharasi (2015) developed a vegetation spectral library for the Arctic, Antarctic, and Chihuahuan Desert using a hand-held portable spectrometer from the visible to near-infrared wavelength range. However, the library only includes data from very limited locations and landcover types. Moreover, in contrast to data acquired in other areas, optical remote sensing data obtained over high-latitude areas that could be utilized in the development of a spectral library are not guaranteed to have radiometric quality because most radiometric calibration and validation work has been carried out in mid-latitude areas. As such, a spectral library for the cold regions is still an unfinished task, but is a fruitful topic for Polar remote sensing studies.

Obtaining field spectra for the development of a spectral library is not easy because they should be measured with several types of ancillary data such as weather condition, solar and sensor geometries, and the distance between the target and sensor. Sun and sensor geometries are especially critical for obtaining accurate and robust spectra. Unfortunately, in the Arctic or Antarctic, very fast changing weather conditions create a major problem that limits the measurement of accurate field spectra. Although a hand-held portable spectrometer may provide more precise spectra for targets and is a popular approach to obtaining field spectra, the risk of using the spectrometer is that the spectra are rarely acquired under the same conditions (e.g., sensor type or resolution) as the image data. Imaging spectrometers such as hyperspectral cameras provide very similar spectral signatures to the RS imagery, but they are spectrally noisy and have relatively low spectral resolution compared to a portable spectrometer.

In this study, a push-broom hyperspectral sensor, which will be mounted on UAVs to collect HSIs over the Polar regions, is used to develop a protocol for collecting library spectra. Because of the difficulties of taking spectra robust to sun and sensor conditions, six laboratory-calibrated targets were used to perform vicarious calibration for obtaining robust spectral signals. Vicarious calibration is often used to perform the absolute radiometric correction of satellite RS data using uniform targets (Dinguirard and Slater, 1999). The hyperspectral sensor used in this study corrects the sensitivity of each detector and converts targets' radiance values to reflectance values using dark and white reference targets, but as shown in Fig. 1, stripes are still remained in the calibrated HSI. Although this is a general approach to converting radiance values to reflectance values, it may not be the best approach to deriving the robust spectra under different lighting and sensor conditions. As shown in Fig. 2, for example,

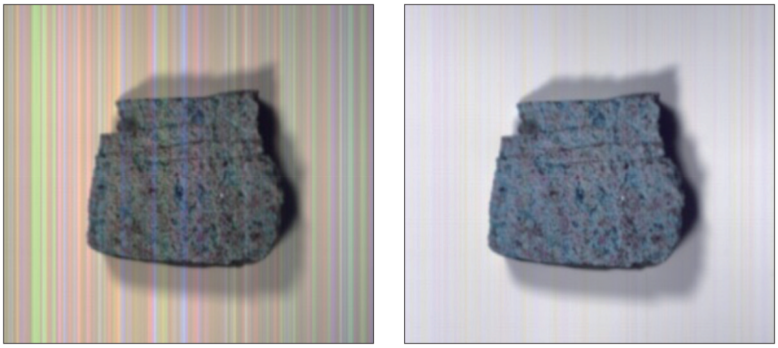

(a) (b)

Fig. 1. Comparison of (a) an uncalibrated raw HSI data and (b) HSI data calibrated by simple built-in software.

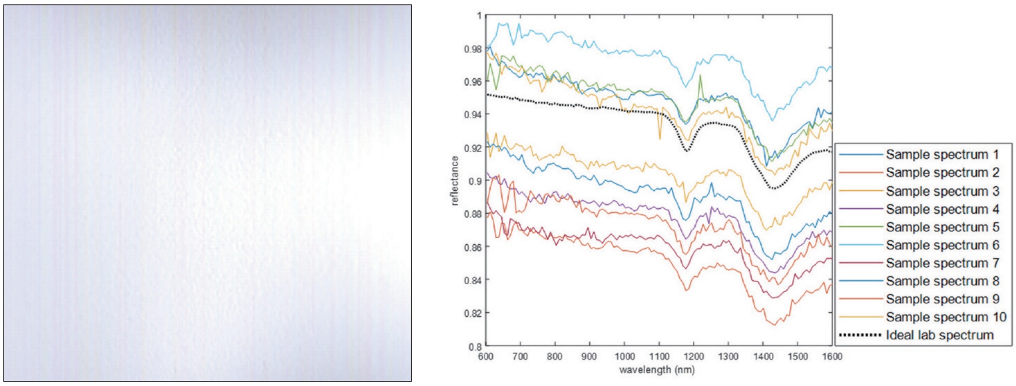


(a) (b)

Fig. 2. (a) HSI data acquired under unstable and nonuniform lighting systems and (b) spectral variations of ten sample spectra derived from the HSI data as well as a spectrum obtained in the laboratory for the same target.

there are differences in the reflectance values of the same target within a homogeneous image because of unstable and nonuniform lighting. The target in Fig. 2(a) is a homogeneous material that has a constant reflectance value, but it seems not to be homogeneous because of nonuniform light sources. Fig. 2(b) shows the spectral variations of ten sample spectra derived from Fig. 2(a) and the lab measured spectrum for the same target. Although the sample spectra have similar absorption features, there are significant spectral variations from the ideal spectrum. This may result in differences and variations in the spectral reflectance values of the spectral library. To always extract the same spectral signals under different conditions for use in a spectral library, this study proposes an approach that uses well-calibrated reference targets and a modified vicarious calibration method. This may help to extract robust spectra using ground-based hyperspectral sensors. These spectra could then be used to develop a spectral library for the Polar regions despite their varying conditions.

## 2. Materials and methods

The hyperspectral data were acquired with a Headwall Photonics Micro-Hyperspec Extended VNIR imager (Headwall Photonics, MA, USA) attached to a motor-operated slider. The sensor is a push-broom scanner, which collects light passing through a lens with an aperture of f/2.8 and then registers the light split into 144 spectral bands of approximately 8-nm width with a digital range of 14-bits and a signal-to-noise ratio (SNR) of 300:1. Because of the low SNR of the short and long wavelengths, the spectral bands of 500-600 nm and 1600-1700 nm were truncated. The HSI system has built-in software to convert radiance values ($L_0$) received the hyperspectral sensor to reflectance values ($\rho$) using

$$\rho = \frac{L_0 - L_D}{L_W - L_D} \tag{1}$$

where $L_W$ and $L_D$ are white and dark reference targets, respectively. However, $\rho$ is a relative value that may not be appropriate for library spectra because $L_D$ and $L_W$ are measured using an uncalibrated hyperspectral sensor and may have different values under different conditions (see Fig. 2). Therefore, $\rho$ shows some linearity with respect to the reflective characteristics of the targets, but may not be used as an absolute reflectance value for a spectral library.

Vicarious calibration is a traditional and common absolute radiometric calibration method for spaceborne sensors. It uses a relationship between digital number (DN) values in an RS image and the corresponding targets' radiance at the sensor ($L$) (Thorne *et al*., 1997; Slater *et al*., 1996). For several reasons such as the absence of an on-board calibrator and the deterioration of the sensor, vicarious calibration is widely used to maintain the radiometric quality of RS images or to derive the absolute radiance or reflectance values. The simple linear relationship between DN and $L$ is defined as

$$L = C_1 \times \mathrm{DN} + C_2 \tag{2}$$

where $C_1$ and $C_2$ are the gain (slope) coefficient and offset value, respectively (Slater *et al*., 1996). This form of the formula is also used in empirical line correction for RS image atmospheric correction, which forces spectral data to match selected field spectra (Karpouzli and Malthus, 2003; Smith and Milton, 1999). As mentioned above, there are variations in spectral responses due to different measurement conditions. To obtain robust spectra, in this study, the equation for vicarious calibration (2) can be phrased using input reflectance ($\rho_1$), which is the relative reflectance value calculated by built-in software, and the calibrated output reflectance ($\rho_2$), which is the absolute and robust value regardless of the measurement environment, as follows:

$$\rho_2 = C_1 \times \rho_1 + C_2 \tag{3}$$

To compute $\rho_2$, uniform radiometric targets that are well calibrated in the laboratory are used.

Reference targets for radiometric calibration must work for a wide range of lighting environments and maintain a uniform spectral reflectance. These targets should also be physically and thermally durable, stable, and have no gloss, polarization, or fluorescence. In this study, six Permaflect radiometric targets (Labsphere, NH, USA) were used to develop vicarious calibration models (in the form of (3)) for HSIs acquired under different lighting conditions. Each target has a constant reflectance value, approximately 94%, 80%, 50%, 18%, 10%, or 5%, across the visible to short-wavelength infrared spectral range (i.e., 400-2500 nm). Fig. 3 presents the six radiometric targets used in this study

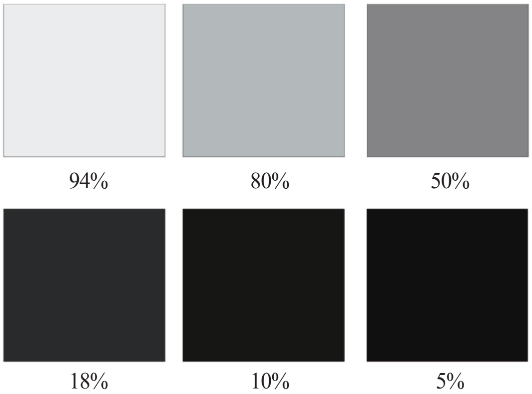


Fig. 3. Six homogeneous reflectance targets used in the study.

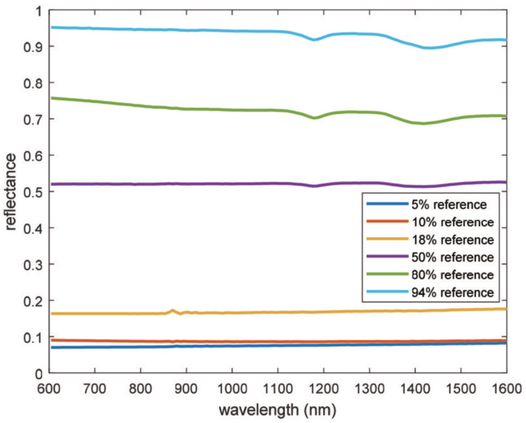


Fig. 4. Spectral reflectance curves of six radiometric targets from 600 to 1600 nm.

and Fig. 4 shows the spectral reflectance curves of the targets measured in the laboratory. Assuming that the lab-spectra of the targets are uniform and do not change, vicarious calibration using these targets was performed to compute the gain and offset coefficients of linear regression models at each pixel location and spectral band. They were then applied to all spectral bands and pixels.

## 3. Experimental results

The aim of this study is to develop a protocol for obtaining robust spectral signals of targets under different lighting conditions that can be utilized in the Polar regions. The HSI system for this study was designed using a motor-operated slider with a motion controller, a height adjusting stage, and two 650-watt halogen lamps (see Fig. 5). Because this is a movable measurement system, the physical position of each part could be different for every measurement. Among the various variables related to measuring conditions such as temperature, light, humidity, and the height of the stage as well as pixel misregistration at subpixel level caused by subtle differences in the exposure time of the motion controller, the amount of light incident on the target may be the most critical cause of spectral variations. To demonstrate this issue, which is related

Fig. 5. Hyperspectral imaging system in this study.

to the low illumination conditions that can occur in the Polar regions, the amount of light illuminating the target is set to 100% (Fig. 6(a)), and then reduced to 30% (Fig. 6(b)). The two HSIs acquired under these different conditions are visually different, as shown in Fig. 6, when only the basic built-in calibration was applied. Although sensitivity correction of the CCD was performed using dark and white references, both HSIs still contain some stripes and the overall color balance between the two images caused by different measurement conditions seems to be corrected before deriving library spectra from the images.

Fig. 7 illustrates an example of the differences in the spectral reflectance curves of selected samples in the two uncalibrated HSIs. Although the spectra of the same material show similar absorption features, each spectrum is positively or negatively shifted depending on the lighting level. For example, the overall reflectance values of the sample spectra 1 and 2 acquired at a lower light level (i.e., 30%) are generally lower than those acquired at the 100% light level, but those of spectra 3 are not. Further, the spectra acquired under low light levels are noisy compared those acquired at full light power, as shown in Fig. 7. These spectral differences might also be caused by subtle changes in the physical position of the light or stage as well as other conditions.

To calibrate the spectra measured under different

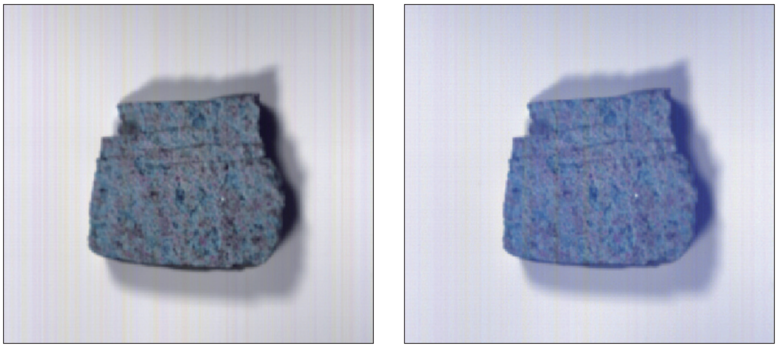

(a) (b)

Fig. 6. HSIs calibrated using basic built-in software acquired at (a) 100% and (b) 30% light levels.

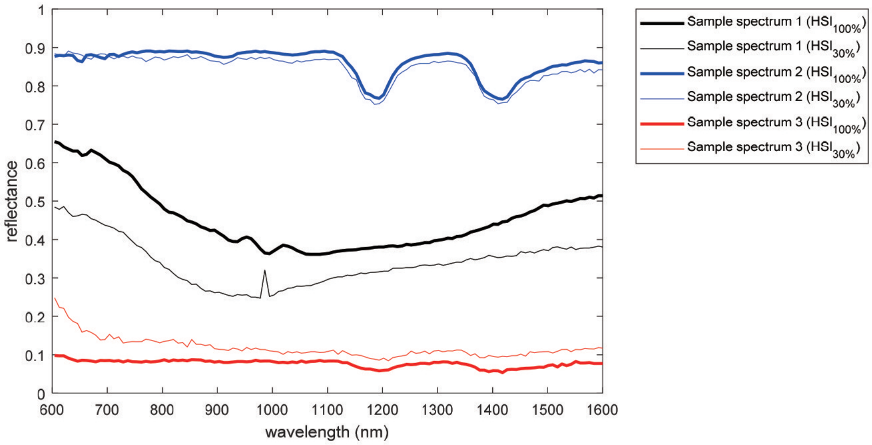


Fig. 7. Comparison of the spectral reflectance curves of sample targets in HSIs acquired at 100% and 30% light levels.

conditions, the six homogeneous radiometric targets presented in Figs. 3 and 4 were used to perform an empirical line correction-based vicarious calibration at each pixel location and each band. Fig. 8 represents an example of the developed linear regression models using the proposed method for two HSIs at the 870 nm wavelength band. The x-axis represents the relative reflectance values of the HSIs ($\rho_1$) that have already been radiometrically corrected by built-in software calibration, and the y-axis shows the absolute reflectance values of the radiometric targets ($\rho_2$) that were measured in the laboratory. Because the relative reflectance values (x-axis) were calculated using dark and white references, both regression models have very high coefficients of determination and show strong linear relationships. Because of the different amount of light incident on the targets, however, the gain and offset values of the regression equations are different, even though both spectra are associated with the same targets. All linear regression equations and r-squared values for each pixel location and each band have been calculated, and Fig. 9 presents the r-squared images at 604 nm and 1592 nm bands. In short wavelength bands, the r-squared values of the regression models are relatively high because of the high spectral irradiance, but they generally decrease in longer wavelength bands because of the low SNR. However, the difference between the best and the worst r-squared values is not significant because in both HSIs, the approximate linearity of the spectral reflectance values is guaranteed

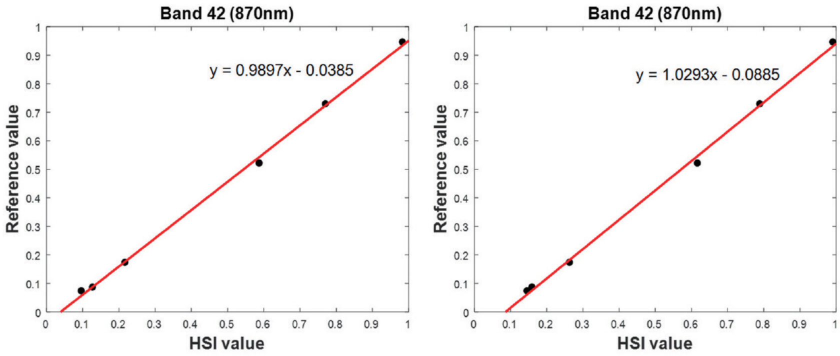


(a) (b)

Fig. 8. Comparison of linear regression models for the 840-nm band of two HSIs acquired at (a) 100% and (b) 30% light levels.

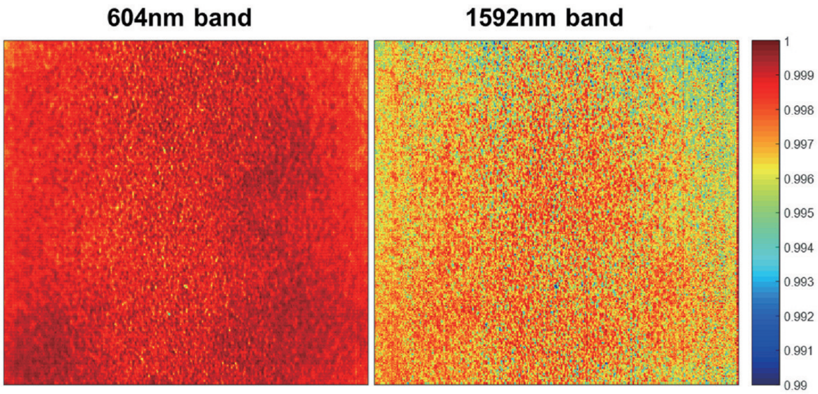


Fig. 9. R-squared images at 640nm and 1592nm bands.

by the built-in software as expected. The regression models developed using the proposed approach are then applied to all spectral bands and all pixels of the HSIs. Fig. 10 shows the resulting HSIs after the proposed calibration method has been applied. Neither image has any stripes due to differences in the CCD sensitivity of noise and are visually identical unlike Fig. 6. Fig. 11 shows the calibrated spectra for the same samples shown in Fig. 7. The calibrated spectra are almost the same regardless of the lighting levels.

Three metrics to quantitatively compute the similarity of two spectra, the Euclidean distance (ED), spectral angle distance (SAD), and normalized cross correlation (NCC), are respectively calculated as follows:

$$\mathrm{ED}(x,y) = \sqrt{\sum_{i=1}^{n}(x_i - y_i)^2} \tag{4}$$

$$\mathrm{SAD}(x,y) = \cos^{-1}\left(\frac{\sum_{i=1}^{n} x_i y_i}{\left(\sum_{i=1}^{n} x_i^2\right)^{\frac{1}{2}} \times \left(\sum_{i=1}^{n} y_i^2\right)^{\frac{1}{2}}}\right) \tag{5}$$

$$\mathrm{NCC}(x,y) = \sum_{i=1}^{n} \frac{(x_i - \mu_x)(y_i - \mu_y)}{\sigma_x \, \sigma_y} \tag{6}$$

where $x$ and $y$ denote uncalibrated spectrum and calibrated spectrum, respectively, $n$ is the number of spectral bands, and $\mu$ and $\sigma$ are the mean and standard deviation of the spectrum, respectively. While the ED shows the differences in the magnitude of two signals,

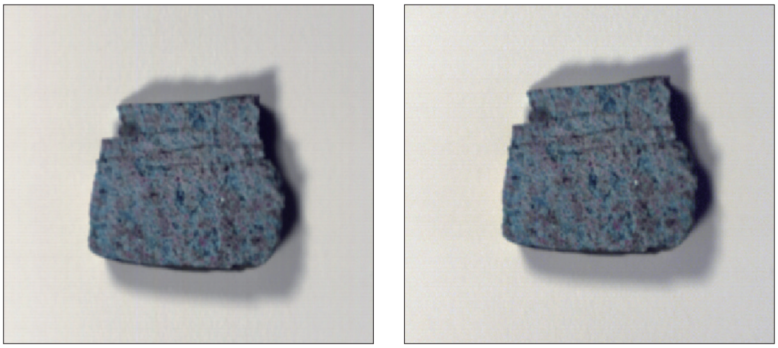

(a) (b)

Fig. 10. Results of full calibration using the proposed method for HSIs acquired at (a) 100% and (b) 30% light levels.

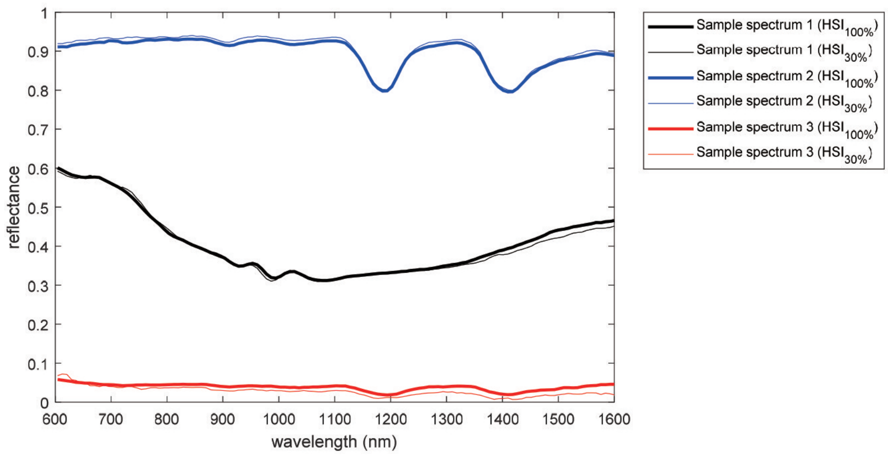


Fig. 11. Comparison of calibrated spectral reflectance curves of sample targets in HSIs acquired at 100% and 30% light levels.

Table 1. Quantitative comparison of spectral similarity of samples

| | Sample 1 | | Sample 2 | | Sample 3 | |
|---|---|---|---|---|---|---|
| | Before calibration | After calibration | Before calibration | After calibration | Before calibration | After calibration |
| ED | 1.3279 | **0.0979** | 0.1979 | **0.1879** | 0.5089 | **0.1428** |
| SAD | 0.0852 | **0.0189** | 0.0101 | **0.0041** | 0.2790 | **0.1632** |
| NCC | 0.8846 | **0.9957** | 0.9723 | **0.9961** | 0.7053 | **0.8471** |

the SAD only examines the similarity of the absorption features of the spectrum (Keshava, 2004). NCC is a widely used metric in signal processing to measure the similarity of two signals as a function of the displacement of one relative to the other (Lewis, 1995). If two spectra are similar, Both the ED and SAD have small values whereas NCC is close to 1. These metrics for the selected samples are listed in Table 1, which shows that all similarity measures yield better values after calibration using the proposed method. The decreased ED and SAD of the samples indicate that the calibrated spectra capture both the overall received energy and the absorption features of the sample spectra, respectively. The NCCs of the calibrated reflectance, which are close to 1, indicate that the similarities of the spectra were quantitatively improved.

Note that the proposed method successfully calibrates spectral reflectance curves acquired under different conditions, and generates robust spectra that can be used for developing a spectral library. Additionally, the proposed method mitigates the impact of noise in the spectra.

## 4. Conclusions

There are several ways to collect the spectral reflectance of ground targets, including airborne/spaceborne RS sensors, field spectrometers, and ground based imaging sensors. In this study, a ground based HSI sensor that will be mounted on a UAV and acquire HSIs over the Polar regions in the near future was used to obtain library spectra. To obtain robust spectra under the fast-changing weather conditions of the Polar regions, this study proposed a new calibration method using a combination of vicarious calibration and multiple targets under different lighting conditions. Although the dark target subtraction-based built-in calibration module of the HSI system itself generated spectra that were somewhat linear and captured absorption features, it resulted in noisy and inconsistent spectra in unstable measurement environments. To address this issue, in this study, six well-calibrated radiometric targets with very consistent spectral characteristics were used to develop vicarious calibration models at each band and pixel location. By applying the developed calibration models, improvements in both statistical and visual quality were achieved. The calibrated spectra were robust to light level and less noisy. Moreover, they captured the absorption features better than the uncalibrated ones.

Successfully obtaining robust spectra from a ground-based HSI sensor has two advantages for data analysis: 1) Image-derived spectra can be collected at the same scale as the image data that will be acquired from the future UAV-mounted system. 2) Image-based library spectra can be more easily associated with features in HSI scenes. Although protocol to obtain robust spectra for the limited samples in this study was proposed, further investigations for a broad range of conditions and targets are needed to develop the final library spectra.

## Acknowledgements

This study was supported by the Korea Polar Research Institute (Grants: Development of hyperspectral remote sensing data acquisition protocol for polar spectral library [PE16410], and Modeling responses of terrestrial organisms to environmental changes on King George Island [PE18090]).

## References

Adams, J. B., M. O. Smith, and P. E. Johnson, 1986. Spectral mixture modeling—A new analysis of rock and soil types at the Viking Lander-1 Site, *Journal of Geophysical Research: Solid Earth*, 91(B8): 8098-8112.

Baldridge, M., S. J. Hook, C. I. Grove, and G. Rivera, 2009. The ASTER spectral library version 2.0, *Remote Sensing of Environment*, 113(4): 711-715.

Chi, J. and M. M. Crawford, 2014. Spectral unmixing-based crop residue estimation using hyperspectral remote sensing data: A case study at Purdue University, *IEEE Journal of Selected Topics in Applied Earth Observations and Remote Sensing*, 7(6): 2531-2539.

Clark, R. N., 1993. Spectroscopy of rocks and minerals, and principles of spectroscopy, *Manual of Remote Sensing*, 3: 3-58.

Clark, R. N., G. A. Swayze, A. J. Gallagher, T.V.V. King, and W. M. Calvin, 1993. *The US Geological Survey, Digital Spectral Library: Version 1 (0.2 to 3.0 um)*, Geological Survey, US.

Dinguirard, M. and P. N. Slater, 1999. Calibration of space-multispectral imaging sensors: A review, *Remote Sensing of Environment*, 68(3): 194-205.

Goswami, S. and K. Matharasi, 2015. Development of a web-based vegetation spectral library (VSL) for remote sensing research and applications, *PeerJ PrePrints*, 3: e915v1.

Green, R. O., B. E. Pavri, and T. G. Chrien, 2003. On-orbit radiometric and spectral calibration characteristics of EO-1 Hyperion derived with an underflight of AVIRIS and in situ measurements at Salar de Arizaro, Argentina, *IEEE Transactions on Geoscience and Remote Sensing*, 41(6): 1194-1203.

Habib, A., W. Xiong, F. He, H. L. Yang, and M. M. Crawford, 2017. Improving orthorectification of UAV-Based push-broom scanner imagery using derived orthophotos from frame cameras, *IEEE Journal of Selected Topics in Applied Earth Observations and Remote Sensing*, 10(1): 262-276.

Habib, A., Y. Han, W. Xiong, F. He, Z. Zhang, and M. M. Crawford, 2016. Automated ortho-rectification of UAV- based hyperspectral data over an agricultural field using frame RGB imagery, *Remote Sensing*, 8(10): 796.

Hruska, R., J. Mitchell, M. Anderson, and N. F. Glenn, 2012. Radiometric and geometric analysis of hyperspectral imagery acquired from an unmanned aerial vehicle, *Remote Sensing*, 4(9): 2736-2752.

Karpouzli, E. and T. Malthus, 2003. The empirical line method for the atmospheric correction of IKONOS imagery, *International Journal of Remote Sensing*, 24(5): 1143-1150.

Keshava, N. and J. F. Mustard, 2002. Spectral unmixing, *IEEE Signal Processing Magazine*, 19(1): 44-57.

Keshava, N., 2004. Distance metrics and band selection in hyperspectral processing with applications to material identification and spectral libraries, *IEEE Transactions on Geoscience and Remote Sensing*, 42(7): 1552-1565.

Lewis, J. P., 1995. Fast template matching, *Proc. of Vision Interface 95*, Quebec City, Canada, May 15-19, pp.120-123.

Martin, M. E. and J. D. Aber, 1997. High spectral resolution remote sensing of forest canopy lignin, nitrogen, and ecosystem processes, *Ecological Applications*, 7(2): 431-443..

Segl, K., L. Guanter, H. Kaufmann, J. Schubert, S. Kaiser, B. Sang, and S. Hofer, 2010. Simulation of spatial sensor characteristics in the context of the EnMAP Hyperspectral Mission, *IEEE Transactions on Geoscience and Remote Sensing*, 48(7): 3046-3054.

Slater, P. N., S. F. Biggar, K. J. Thome, D. I. Gellman, and P. R. Spyak, 1996. Vicarious radiometric calibrations of EOS sensors, *Journal of Atmospheric and Oceanic Technology*, 13(2): 349-359.

Smith, G. M. and E. J. Milton, 1999. The use of the empirical line method to calibrate remotely sensed data to reflectance, *International Journal of Remote Sensing*, 20(13): 2653-2662.

Solomon, J. and B. Rock, 1985. Imaging spectrometry for earth remote sensing, *Science*, 228(4704): 1147-1153.

Thorne, K., B. Markharn, and P. S. Barker, 1997. Radiometric calibration of Landsat, *Photogrammetric Engineering & Remote Sensing,* 63(7): 853-858.